Diode-pumped visible lasing in femtosecond-laser-written Pr:$LiLuF_4$ waveguide

DAVIDE BAIOCCO[1,*], IGNACIO LOPEZ-QUINTAS[2], JAVIER R. VÁZQUEZ DE ALDANA[2], MAURO TONELLI[1], AND ALESSANDRO TREDICUCCI[1]

[1] Dipartimento di Fisica, Università di Pisa, Largo Bruno Pontecorvo 3, 56127 Pisa PI, Italy
[2] Grupo de Investigación en Aplicaciones del Láser y Fotónica, Universidad de Salamanca, Pl. La Merced SN. 37008 Salamanca, Spain
[*] Corresponding author:davide.baiocco@phd.unipi.it

Compiled March 3, 2023

In this Letter we report the realization of a femtosecond-laser-written diode-pumped Pr:$LiLuF_4$ visible waveguide laser. The waveguide studied in this work consisted of a depressed-index cladding, whose design and fabrication were optimized to minimize the propagation loss. Laser emission has been achieved at 604 nm and 721 nm , with output power of 86 mW and 60 mW respectively and slope efficiencies of 16% and 14%. In addition, we obtained, for the first time in a praseodymium-based waveguide laser, stable continuous-wave laser operation at 698 nm (3 mW of output power and 0.46% of slope efficiency), corresponding to the wavelength necessary for the clock transition of the strontium-based atomic clock. The waveguide laser emission at this wavelength is mainly in the fundamental mode (i.e. the larger propagation constant mode) showing a nearly gaussian intensity profile.

http://dx.doi.org/10.1364/ao.XX.XXXXXX

The necessity for miniaturized optical devices led to the search for compact laser sources emitting in the visible range. A common solution is to employ laser diodes, but these devices have some undesired characteristics as, for example, a poor beam quality and the presence of aging effects and frequency runaway [1]. Another class of durable and stable laser emitters are solid state lasers (SSLs). SSLs possess emission regions often not covered by laser diodes and are stable, have quasi-diffraction limited output beam, and do not show the aforementioned aging effects, making them ideal for long term and aerospace applications. In addition, SSLs have the advantage of a narrower emission bandwidth, which translates in a greater frequency stability, with respect to laser diodes, an important feature for metrological applications. Moreover, the invention and the availability of Watt-level InGaN-based laser diodes allows the development of inexpensive and compact diode-based optical pumping setups for SSLs [2]. An interesting ion that has been successfully employed in SSLs operating in the visible spectrum is praseodymium. This ion possesses absorption lines in the emission band of InGaN-based laser diodes (approx. 445 nm) and a fluorescence spectrum with lines in all the visible spectrum, from cyan, 480 nm, to deep red, 720 nm [3].

Praseodymium-doped fluoride crystals have proven to be an optimal platform for the development of high-efficiency visible laser sources [2]. Indeed, these crystals possess a lower crystal field strength, which translates into a reduction of excited state absorption to the 5d excited levels of Pr^{3+} [2], and a lower effective phonon energy with respect to oxides, corresponding to lower phonon-induced decay of the upper laser levels of Pr^{3+} ions [3, 4]. Both these effects lead to better laser performance. In addition, fluoride crystals have the advantage of being chemically stable and relatively not hygroscopic, making them suitable for the fabrication of devices, especially those requiring long-lasting performance. Another interesting feature of the Pr^{3+} emission spectrum is that, if embedded in fluoride crystals, it includes all the lines necessary for strontium-based optical atomic clocks [5]. These lines are, for example, 689 nm and 698 nm, employed for cooling and clock in neutral strontium atoms.

SSLs usually employ an external cavity to achieve lasing. In the years, many techniques were tested to fabricate more compact and lightweight SSLs. Davis et al. [6] demonstrated that it is possible to produce a localized refractive index change in a transparent dielectric by direct irradiation with a focused femtosecond laser pulse, opening the door to the fabrication of 3D optical waveguides in the bulk of a target host. Since then, many works have been published, reporting the operation of waveguide laser in the range 1 µm-2 µm, using as active ion Nd^{3+}, Tm^{3+} or Yb^{3+}, [7–11], only to cite a few examples. On the contrary, only few results regarding praseodymium-based visible waveguide lasers have been published [4, 12–16], mainly due to the difficulty of obtaining such materials with low phonon energy and a waveguide with low propagation losses in the visible range. Laser emission in waveguides offers several advantages compared to bulk emission, i.e. lower lasing threshold, the possibility of beam shape control and integration in complex 3D photonic devices.

In this Letter we report, for the first time to the best of our knowledge, the operation of a femtosecond-laser-written waveguide laser based on Pr:$LiLuF_4$ (Pr:LLF). Laser emission has been achieved at 604 nm, 721 nm and, for the first time in a waveguide laser, 698 nm, corresponding to the line necessary for the operation of strontium-based atomic clock.

To fabricate a praseodymium-based waveguide laser by direct femtosecond-laser irradiation we employ lithium lutetium fluoride, $LiLuF_4$ (LLF), as host. LLF is a tetragonal crystal, $a = 5.124$ Å $c = 10.54$ Å, with a scheelite-like structure and it is thus isomorph to $LiYF_4$ [17] but shows better properties in terms of crystal growth and thermomechanical properties with respect to YLF [18]. In this host, the Pr^{3+} absorption line lies at 444 nm for π polarization (E//c). The emission spectrum covers all the visible range and depends on the polarization of the emitted radiation. The π-polarized fluorescence spectrum of Pr:LLF for the 600-750 nm spectral range is composed by three main peaks: 604 nm ($^3P_0 \rightarrow ^3H_6$), 698 nm ($^3P_0 \rightarrow ^3F_3$) and 721 nm ($^3P_0 \rightarrow ^3F_4$). Absorption and fluorescence spectra can be found in [3].

For the experiments, monocrystalline $LiLuF_4$:Pr was grown at University of Pisa in a Czochralski furnace from LiF, LuF_3 and PrF_3 high purity powders [3]. The nominal doping in the melt was 1%. The obtained boule was oriented through X-ray backscattering Laue technique in order to identify crystallographic axes and produce an a-cut oriented sample. Subsequently the crystal was polished to obtain laser-quality optically flat facets. Final sample dimensions are 4 mm(a)×4 mm(c)×8 mm(a). Due to the segregation effects [3], the dopant concentration in the crystal is different from the nominal doping in the melt. Measuring the absorption coefficient, the effective Pr concentration can be determined by knowing the absorption cross sections of Pr^{3+} ions, reported in [2]. The absorption measurement was carried out using a CARY 5000 spectrophotometer. The effective dopant concentration is estimated to be 0.2%.

The fabrication of the waveguides was done in the Laser Laboratory at the University of Salamanca. We used an amplified Ti:Sapphire laser system (Spitfire ACE, Spectra Physics) that delivers 60 fs pulses with a central wavelength of 800 nm at a repetition rate of 5 kHz. The pulse energy was finely controlled by a set of half-wave plate and a linear polarizer, followed by a calibrated neutral density filter. Then, the beam was focused by a 40× microscope objective (Leica N-PLAN, N.A. 0.60) through the sample surface (c-cut facet), while it was moved by a motorized XYZ micro-positioning stage in order to obtain 8 mm long structures.

For both transmission and laser experiments, the crystal was placed in a copper holder connected to a thermoelectric cooler (TEC) which allows cooling and temperature stabilization of the sample through a custom-made setup. Different strategies [19] were tested for waveguide inscription in the Pr:LLF sample.

Efficient structures were obtained based on both type-I (weak) and type-II (severe) material modifications. In particular, depressed-index cladding waveguides were designed and fabricated with different geometries, such as circular claddings, improved circular claddings [20] or hexagonal claddings; a comparative study will be presented elsewhere. In this manuscript, we analyzed in detail the best results, obtained with a depressed-index cladding waveguide, designed to exhibit very low propagation loss. It consisted of a tubular structure (radius of 20 microns) defined by parallel damage tracks with maximum separation of 2 µm between them, and a set of additional tracks at the sides, forming an "ear-like" structure. This kind of design, even though it only supports leaky modes [21], has been demonstrated to produce very good performance for waveguide lasers inscribed in other host materials [20]. For the fabrication of the waveguide, the pulse energy was set to 70 nJ and the scanning velocity was 0.60 mm/s.

A microscope picture of the waveguide cross section is shown in Fig. 1. The measured horizontal radius is 19.6 µm and the vertical one is 20.0 µm. The coupling and transmission of polarized radiation in the waveguide was explored. For that purpose, the whole system was placed on a XYZ translation stage with a 3-axes goniometer. A first optical characterization was performed at 632.8 nm with a He-Ne laser. Several coupling lenses have been tried in order to find the best performance, which was obtained with a 30 mm focal length aspherical lens. As collection optics, an OLYMPUS PLN20× microscope objective with N.A. of 0.4 was employed, image-forming the intensity profile of the mode of the waveguide on a beam profiler (BP, DataRay WinCamD-UCD15). To control the positions of the optics, both the coupling and the collection optics were placed on two 3D precision translation stages (THORLABS MBT616D/M). The waveguide shows very good confinement for π-polarization, as can be seen in Fig. 1, but shows very weak coupling of σ-polarization (E//a) in the tracks which constitute the cladding: this behavior is similar to that reported for cladding structures in $Pr:LiYF_4$ [15]. The large size of the waveguide radius reflects in a multimodal behaviour at visible wavelengths. The intensity profile reported in figure 1 was acquired for the input alignment condition at which the maximum output power was obtained. To evaluate the propagation loss, input and output powers were measured and, after subtraction of the Fresnel reflection losses and the optics losses, an upper limit of 0.12 dB/cm can be set for π-polarization (assuming the complete coupling of the incident radiation in the waveguide). This value is much smaller than most of the previously reported femtosecond-laser written waveguides in fluoride crystals, [13–15], and is similar to the value reported in [16] for ultra-large area waveguides fabricated with the helical inscription technique. For σ polarization, the corresponding upper limit is about 15 dB/cm. Finally, by measuring the divergence of the output beam, it was possible to estimate the reduction of refractive index at the damage tracks due to the writing procedure, through the step-index waveguide approximation [8], resulting in a $\Delta n = -2 \cdot 10^{-4}$ at 632.8 nm.

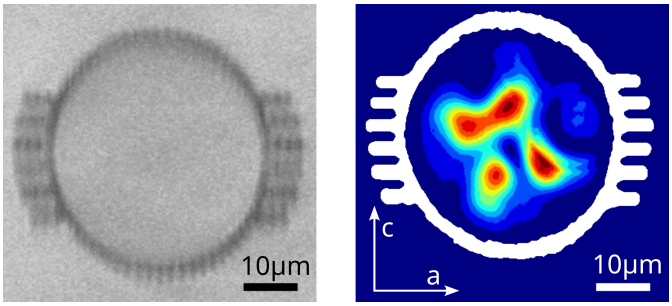

Fig. 1. Microscope image (left) and intensity profile of the $\pi-$polarized guided mode at 632.8 nm (right) for the waveguide analyzed in this Letter.

Lasing of the waveguide was studied by pumping with an InGaN-based laser diode, tuned to emit at 444 nm, in order to match the absorption peak of Pr^{3+} ions. The beam was collected through a collimation lens followed by a couple of cylindrical lenses (Schäfter+Kirchhoff 5 AN-3-V-35), used to reduce the beam astigmatism. Since the laser diode emission is polarized, an half wavelength plate and a polarizing beam splitter were used to regulate the pump beam power. A second half wavelength plate was inserted to adjust the polarization of the pump beam, in order to study the propagation of both π-polarization

and σ-polarization at 444 nm. The maximum available power after all these optical elements was about 1.7 W. The pump beam was focused with an aspherical lens of 30 mm of focal length. The focused beam was studied with the BP and has a waist diameter of 60 µm in the horizontal direction and 40 µm in the vertical direction. The corresponding value of M_x^2 (horizontal direction) is 20 and M_y^2 is 1.7 (vertical direction). The definitions employed for M_x^2 and M_y^2 are those indicated in ISO 11146-1:2021 standard.

Due to the saturation of pump absorption, phenomenon observed also in [8], coupling efficiency can be measured comparing the transmitted power with different incident power, resulting in a value of $(44 \pm 2)\%$ for π-polarization, the one of interest for optical pumping of Pr^{3+} ions. The same 30 mm-focal-length lens was chosen for the laser experiments because it allows the highest coupling efficiency of the pump beam in the waveguide, resulting in the best compromise between waist diameter and beam divergence, which must be limited due to the numerical aperture of the waveguide (N.A.$\approx$ 0.03). Since the pump coupling efficiency has been measured, both the threshold power (P_{TH}) and the slope efficiency ($\eta_C = \frac{dP_{OUT}}{dP_c}$), will be given with respect to the power coupled in the waveguide (P_c). Here P_{OUT} is the laser output power.

The laser cavity was made by two plane mirrors, fig. 2. The pump mirror is highly reflective at the laser wavelengths (T=0.1% at 604 nm and T<10^{-5} for 698 nm and 721 nm) and possesses high transmittance (T>98%) at the pump wavelength. Different output couplers (OCs) were used to obtain laser operation at the different wavelengths. Each mirror was installed in a two-axes mount that allows fine tilt adjustment. The mount was fixed over a 3D translation stage, allowing thus the positioning of the mirrors butt-coupled to the crystal facets. An aspherical lens of focal length of 20 mm was used to collect the laser emission and a 510 nm long-pass dielectric filter was used to remove the residual pump. The laser intensity profiles were registered with the BP placed in the conjugated plane of the waveguide output. During laser experiments, the temperature of the sample was maintained at 12 °C to maximize the cooling of the crystal while avoiding moisture condensation on the sample. The whole setup is schematized in fig. 2.

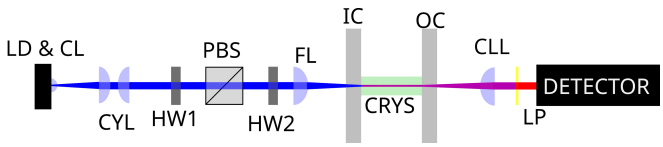

Fig. 2. Schematics of the laser setup. LD: laser diode, CL: collimation lens, CYL: cylindrical lenses, HW1 and HW2: half-wavelength plate, PBS: polarizing beam splitter, FL: focusing lens, IC: input coupler, CRYS: crystal, OC: output coupler, CLL: collection lens, LP: long pass dielectric filter.

Laser emission was achieved from the waveguide presented in this Letter and the laser emission spectrum was acquired using a QEpro spectrometer (resolution of about 1 nm).

For the orange (604 nm), a mirror with a transmission of 17% at 604 nm was used. The maximum output power obtained was 86 mW with η_c equal to 16% and P_{TH} of 100 mW. To achieve lasing at 721 nm, the chosen mirror had a transmission of 46% at 721 nm and 96% at 604 nm, in order to suppress parasitic lasing at this wavelength. The maximum output power was 60 mW, η_c was 14% and P_{TH} was equal to 280 mW. Data and linear fit for both laser wavelengths are reported in fig. 3, where are also shown the intensity profiles of laser emissions as insets. The presence of multiple lobes is due to the multimodal nature of the waveguide and the shape of the output beam depends on the pump alignment. The intensity profiles were collected at maximum output power and are stable reducing the pump power. Finally, to operate the laser at 698 nm a mirror with 0.03%

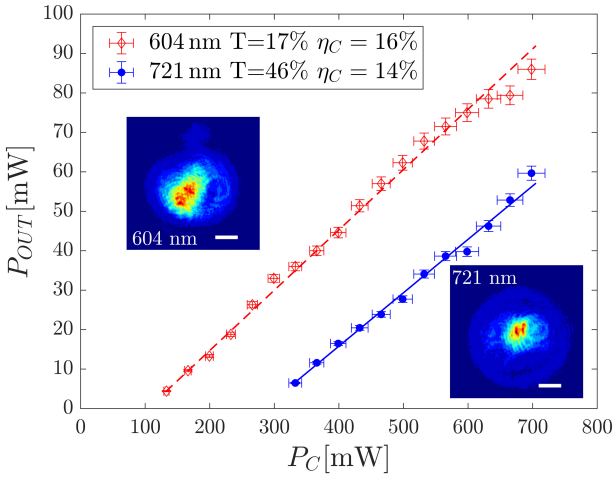

Fig. 3. Data and linear fit for 604 nm (P_{TH} equal to 100 mW) and 721 nm (P_{TH} of 280 mW) wavelength. P_c is the pump power coupled in the waveguide while P_{OUT} is the laser output power. The scale bar in the intensity profiles corresponds to 20 µm.

transmission at this wavelength was used, while its transmission at 604 nm and 721 nm is 77% and 0.05% respectively. The maximum power obtained is 3 mW while η_c is 0.46% and P_{TH} is 25 mW. Data and linear fit are shown in fig. 4. The low transmission of the OC, compared to those employed for the other two lines, is due to the lower emission cross section of the $^3P_0 \rightarrow {}^3F_3$ transition [2] with respect to that of $^3P_0 \rightarrow {}^3F_4$ transition. This leads to the difficulty of obtaining free running laser emission at this wavelength with a broadband mirror, owing to the competition with a transition of larger emission cross section. All the laser emissions obtained are π-polarized.

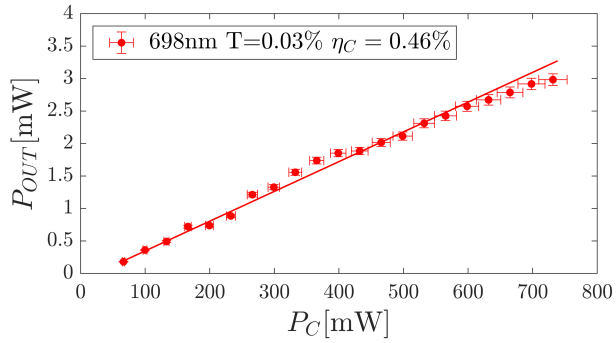

Fig. 4. Data and linear fit for 698 nm wavelength. (P_{TH} is equal to 25 mW) P_c is the pump power coupled in the waveguide while P_{OUT} is the laser output power.

As it can be seen in Fig. 5, the waveguide laser at 698 nm exhibited a very good intensity profile, constituted by a single lobe, resembling a nearly gaussian mode. The values of M_x^2 and

M_y^2 were measured by studying the laser beam focused by an aspherical lens. The obtained values are 1.5(x) and 1.9(y). This different behavior between the two axes can be understood in terms of the different refractive index profile of the waveguide along both axes due to the processing geometry, as well as due to the presence of defects along the tracks produced during the fabrication process. To fully understand this result, we performed numerical simulations of the waveguide fundamental mode by solving the wave-equation and taking as input parameter the refractive index decrease reported previously ($\Delta n = 2 \cdot 10^{-4}$). The solving method that we used was the imaginary distance beam propagation method implemented on a finite difference scheme of the wave equation [22]. The simulated index profile and the obtained mode are shown in Fig. 5, where a fairly good agreement between measured and reconstructed modal profiles is shown. It is important to notice that even though the waveguide shows many leaky modes in the visible, it is possible to get laser emission just in a single mode, making it much more convenient for any practical application of the laser.

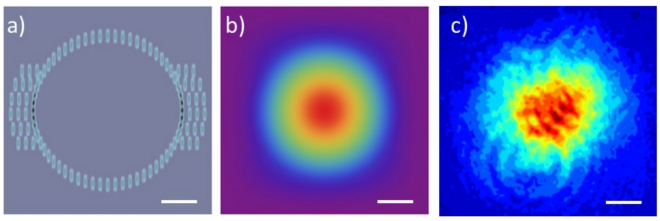

Fig. 5. a) Refractive-index profile used in the numerical simulations. b) Calculated intensity profile for the fundamental mode at 698 nm. c) Measured intensity profile of the waveguide laser at 698 nm. The scale bar corresponds to 10 µm.

In conclusion, we reported the fabrication of the first Pr:LLF based waveguide laser operating in the visible range. An optimized-design optical waveguide was fabricated by femtosecond laser direct inscription in a depressed-cladding configuration, showing propagation loss as low as 0.12 dB/cm. Lasing was achieved at 604 nm and 721 nm, with output power greater than those reported for Pr:YLF-based waveguide lasers employing waveguides of comparable dimension [14, 15]. This result was reached using high quality materials and a carefully designed low-loss waveguide. Employing ultra-large area waveguides, higher output power can be obtained, at least for the $^3P_0 \rightarrow {}^3H_6$ transition, but with a worse quality emission mode [16]. Finally, we realized for the first time a waveguide laser operating at 698 nm, corresponding to the line required for the strontium-based atomic clock, where a few milliwatts are sufficient for the clock transition [23]. The low emitted power achieved at 698 nm could be justified by the low transmission of the OC at this wavelength. In future experiments, a specifically designed mirror could prevent parasitic lasing at the other two wavelengths, while enhancing emission at the desired one. Miniaturization and stabilization of the whole system can be reached substituting the mirrors with reflective coatings, obtaining thus a compact and lightweight monolithic system with a greater overlap efficiency between the pump mode and the laser mode due to the lateral confinement provided by the waveguide. Despite the current low output power with respect to laser results obtained with the same active materials [2], this type of approach offers interesting perspectives in developing small and compact coherent devices with reduced frequency noise when compared to classical laser devices, where refractive elements such as etalons and birefringent plates are present and cause this type of noise. This opens up interesting metrological applications for ultra-stable sources where powers of tens of milliwatts are sufficient.

Funding. Consejería de Educación, Junta de Castilla y León (SA136P20); Ministerio de Ciencia, Innovación y Universidades (PID2020-119818);

Acknowledgments. The authors would like to acknowledge E. Damiano, G. Cittadino and F. Caminati for the helpful discussions.

Disclosures. The authors declare no conflicts of interest.

Data availability. Data underlying the results presented in this paper are not publicly available at this time but may be obtained from the authors upon reasonable request.

REFERENCES

1. R. Matthey, C. Affolderbach, and G. Mileti, Opt. Lett. **36**, 3311 (2011).
2. C. Kränkel, D.-T. Marzahl, F. Moglia, G. Huber, and P. W. Metz, Laser & Photonics Rev. **10**, 548 (2016).
3. F. Cornacchia, A. Richter, E. Heumann, G. Huber, D. Parisi, and M. Tonelli, Opt. Express **15**, 992 (2007).
4. T. Calmano, J. Siebenmorgen, F. Reichert, M. Fechner, A.-G. Paschke, N.-O. Hansen, K. Petermann, and G. Huber, Opt. Lett. **36**, 4620 (2011).
5. A. Sottile, E. Damiano, A. D. Lieto, and M. Tonelli, Opt. Lett. **44**, 594 (2019).
6. K. M. Davis, K. Miura, N. Sugimoto, and K. Hirao, Opt. Lett. **21**, 1729 (1996).
7. Y. Morova, M. Tonelli, and A. Sennaroglu, Opt. Mater. **126**, 112121 (2022).
8. E. Kifle, P. Loiko, X. Mateos, J. R. V. de Aldana, A. Ródenas, U. Griebner, V. Petrov, M. Aguiló, and F. Díaz, Opt. Mater. Express **7**, 4258 (2017).
9. A. G. Okhrimchuk, A. V. Shestakov, I. Khrushchev, and J. Mitchell, Opt. Lett. **30**, 2248 (2005).
10. A. Okhrimchuk, V. Mezentsev, A. Shestakov, and I. Bennion, Opt. express **20**, 3832 (2012).
11. T. Calmano, A.-G. Paschke, S. Müller, C. Kränkel, and G. Huber, Opt. Express **21**, 25501 (2013).
12. F. Reichert, T. Calmano, S. Müller, D.-T. Marzahl, P. W. Metz, and G. Huber, Opt. Lett. **38**, 2698 (2013).
13. T. Calmano, A. Sottile, P. W. Metz, D. Parisi, C. Kränkel, M. Tonelli, and G. Huber, "Ultrafast Laser Inscribed Pr:KY3F10 Waveguides for Dual Wavelength and Switchable Waveguide Lasers in the Visible," in *Advanced Solid State Lasers,* (Optica Publishing Group, 2015), p. AW1A.5.
14. H. Liu, S. Luo, B. Xu, H. Xu, Z. Cai, M. Hong, and P. Wu, Opt. Mater. Express **7**, 3990 (2017).
15. S. Müller, T. Calmano, P. Metz, N.-O. Hansen, C. Kränkel, and G. Huber, Opt. Lett. **37**, 5223 (2012).
16. Y. Ren, Z. Cui, L. Sun, C. Wang, H. Liu, and Y. Cai, Chin. Opt. Lett. **20**, 122201 (2022).
17. A. A. Kaminskii, K. ichi Ueda, and N. Uehara, Jpn. J. Appl. Phys. **32**, L586 (1993).
18. R. L. Aggarwal, D. J. Ripin, J. R. Ochoa, and T. Y. Fan, J. Appl. Phys. **98**, 103514 (2005).
19. F. Chen and J. R. V. de Aldana, *Direct Femtosecond Laser Writing of Optical Waveguides in Dielectrics* (Springer International Publishing, Cham, 2020), pp. 185–210.
20. X. Sun, S. Sun, C. Romero, J. R. V. de Aldana, F. Liu, Y. Jia, and F. Chen, Opt. Express **29**, 4296 (2021).
21. J. Hu and C. R. Menyuk, Adv. Opt. Photon. **1**, 58 (2009).
22. Y. Tsuji and M. Koshiba, J. Light. Technol. **18**, 618 (2000).
23. Y.-B. Wang, M.-J. Yin, J. Ren, Q.-F. Xu, B.-Q. Lu, J.-X. Han, Y. Guo, and H. Chang, Chin. Phys. B **27**, 023701 (2018).

FULL REFERENCES

1. R. Matthey, C. Affolderbach, and G. Mileti, "Methods and evaluation of frequency aging in distributed-feedback laser diodes for rubidium atomic clocks," Opt. Lett. **36**, 3311–3313 (2011).
2. C. Kränkel, D.-T. Marzahl, F. Moglia, G. Huber, and P. W. Metz, "Out of the blue: semiconductor laser pumped visible rare-earth doped lasers," Laser & Photonics Rev. **10**, 548–568 (2016).
3. F. Cornacchia, A. Richter, E. Heumann, G. Huber, D. Parisi, and M. Tonelli, "Visible laser emission of solid state pumped LiLuF4:Pr3+," Opt. Express **15**, 992–1002 (2007).
4. T. Calmano, J. Siebenmorgen, F. Reichert, M. Fechner, A.-G. Paschke, N.-O. Hansen, K. Petermann, and G. Huber, "Crystalline Pr:SrAl12O19 waveguide laser in the visible spectral region," Opt. Lett. **36**, 4620–4622 (2011).
5. A. Sottile, E. Damiano, A. D. Lieto, and M. Tonelli, "Diode-pumped solid-state laser platform for compact and long-lasting strontium-based optical clocks," Opt. Lett. **44**, 594–597 (2019).
6. K. M. Davis, K. Miura, N. Sugimoto, and K. Hirao, "Writing waveguides in glass with a femtosecond laser," Opt. Lett. **21**, 1729–1731 (1996).
7. Y. Morova, M. Tonelli, and A. Sennaroglu, "Fabrication of femtosecond laser written depressed-cladding waveguides in Tm3+:BaY2F8 crystal and laser operation near 2μm," Opt. Mater. **126**, 112121 (2022).
8. E. Kifle, P. Loiko, X. Mateos, J. R. V. de Aldana, A. Ródenas, U. Griebner, V. Petrov, M. Aguiló, and F. Díaz, "Femtosecond-laser-written hexagonal cladding waveguide in Tm:KLu(WO4)2: µ-Raman study and laser operation," Opt. Mater. Express **7**, 4258–4268 (2017).
9. A. G. Okhrimchuk, A. V. Shestakov, I. Khrushchev, and J. Mitchell, "Depressed cladding, buried waveguide laser formed in a YAG:Nd3+ crystal by femtosecond laser writing," Opt. Lett. **30**, 2248–2250 (2005).
10. A. Okhrimchuk, V. Mezentsev, A. Shestakov, and I. Bennion, "Low loss depressed cladding waveguide inscribed in YAG: Nd single crystal by femtosecond laser pulses," Opt. express **20**, 3832–3843 (2012).
11. T. Calmano, A.-G. Paschke, S. Müller, C. Kränkel, and G. Huber, "Curved Yb:YAG waveguide lasers, fabricated by femtosecond laser inscription," Opt. Express **21**, 25501–25508 (2013).
12. F. Reichert, T. Calmano, S. Müller, D.-T. Marzahl, P. W. Metz, and G. Huber, "Efficient visible laser operation of Pr,Mg:SrAl12O19 channel waveguides," Opt. Lett. **38**, 2698–2701 (2013).
13. T. Calmano, A. Sottile, P. W. Metz, D. Parisi, C. Kränkel, M. Tonelli, and G. Huber, "Ultrafast Laser Inscribed Pr:KY3F10 Waveguides for Dual Wavelength and Switchable Waveguide Lasers in the Visible," in *Advanced Solid State Lasers,* (Optica Publishing Group, 2015), p. AW1A.5.
14. H. Liu, S. Luo, B. Xu, H. Xu, Z. Cai, M. Hong, and P. Wu, "Femtosecond-laser micromachined Pr:YLF depressed cladding waveguide: Raman, fluorescence, and laser performance," Opt. Mater. Express **7**, 3990–3997 (2017).
15. S. Müller, T. Calmano, P. Metz, N.-O. Hansen, C. Kränkel, and G. Huber, "Femtosecond-laser-written diode-pumped Pr:LiYF4 waveguide laser," Opt. Lett. **37**, 5223–5225 (2012).
16. Y. Ren, Z. Cui, L. Sun, C. Wang, H. Liu, and Y. Cai, "Laser emission from low-loss cladding waveguides in pr:ylf by femtosecond laser helical inscription," Chin. Opt. Lett. **20**, 122201 (2022).
17. A. A. Kaminskii, K. ichi Ueda, and N. Uehara, "New Laser-Diode-Pumped CW Laser Based on Nd^{3+}-Ion-Doped Tetragonal $LiLuF_4$ Crystal," Jpn. J. Appl. Phys. **32**, L586–L588 (1993).
18. R. L. Aggarwal, D. J. Ripin, J. R. Ochoa, and T. Y. Fan, "Measurement of thermo-optic properties of Y3Al5O12, Lu3Al5O12, YAlO3, LiYF4, LiLuF4, BaY2F8, KGd(WO4)2, and KY(WO4)2 laser crystals in the 80–300K temperature range," J. Appl. Phys. **98**, 103514 (2005).
19. F. Chen and J. R. V. de Aldana, *Direct Femtosecond Laser Writing of Optical Waveguides in Dielectrics* (Springer International Publishing, Cham, 2020), pp. 185–210.
20. X. Sun, S. Sun, C. Romero, J. R. V. de Aldana, F. Liu, Y. Jia, and F. Chen, "Femtosecond laser direct writing of depressed cladding waveguides in Nd:YAG with "ear-like"; structures: fabrication and laser generation," Opt. Express **29**, 4296–4307 (2021).
21. J. Hu and C. R. Menyuk, "Understanding leaky modes: slab waveguide revisited," Adv. Opt. Photon. **1**, 58–106 (2009).
22. Y. Tsuji and M. Koshiba, "Guided-mode and leaky-mode analysis by imaginary distance beam propagation method based on finite element scheme," J. Light. Technol. **18**, 618 (2000).
23. Y.-B. Wang, M.-J. Yin, J. Ren, Q.-F. Xu, B.-Q. Lu, J.-X. Han, Y. Guo, and H. Chang, "Strontium optical lattice clock at the national time service center," Chin. Phys. B **27**, 023701 (2018).